applied sciences

IMPACT FACTOR 2.5

CITESCORE 5.5

Article

Selective Laser-Melted Alloy 625: Optimization of Stress-Relieving and Aging Treatments

Barbara Rivolta, Riccardo Gerosa and Davide Panzeri

Special Issue

Machine Tools, Advanced Manufacturing and Precision Manufacturing

Edited by

Dr. Abhilash Puthanveettil Madathil and Prof. Dr. Xichun Luo

MDPI

https://doi.org/10.3390/app15105441

applied sciences

MDPI

Article

Selective Laser-Melted Alloy 625: Optimization of Stress-Relieving and Aging Treatments

Barbara Rivolta *, Riccardo Gerosa and Davide Panzeri

Department of Mechanical Engineering, Politecnico di Milano, via La Masa 1, 20133 Milan, Italy; riccardo.gerosa@polimi.it (R.G.); davide.panzeri@polimi.it (D.P.)
* Correspondence: barbara.rivolta@polimi.it

Abstract: Additive manufacturing is an innovative solution to produce components characterized by complex geometries. The use of such parts requires a deep knowledge of their behavior under different service conditions, especially from mechanical and corrosion resistance points of view. One of the most well-known and employed materials produced by selective laser melting is nickel alloy 625. It is already commonly used in its conventional form, but the additive manufacturing technology, despite its higher production costs and lower productivity, is becoming competitive because of its excellent mechanical strength. It is in fact significantly higher compared to the conventionally manufactured alloy whose properties are often limited by the difficulty in retaining a fine grain size during plastic deformation and heat treatment. Even though the as-built performance is already quite good, further strength improvement can be attained upon tailored single- and double-aging treatments that are optimized starting from the experimental results obtained in the conventional alloy and also considering the influence on corrosion resistance. In addition, considering that the stress-relieving treatment recommended for the conventional forged alloy at 870 °C is not suitable for the selective laser-melted material because of the more rapid precipitation response, this temperature is optimized to improve both the tensile deformability and the corrosion behavior.

Keywords: alloy 625; selective laser melting; aging treatment; stress-relieving treatment; corrosion resistance

Academic Editors: Abhilash Puthanveettil Madathil and Xichun Luo

Received: 10 April 2025
Revised: 7 May 2025
Accepted: 9 May 2025
Published: 13 May 2025

Citation: Rivolta, B.; Gerosa, R.; Panzeri, D. Selective Laser-Melted Alloy 625: Optimization of Stress-Relieving and Aging Treatments. *Appl. Sci.* **2025**, *15*, 5441. https://doi.org/10.3390/app15105441

1. Introduction

Nickel alloy 625 was patented in 1964 by H. L. Eiselstein and J. Gadbut. Its chemical composition is characterized by the presence of high amounts of chromium, molybdenum, and niobium, which provide excellent mechanical strength and corrosion resistance in several environments [1–11]. For such a reason, this alloy grade is adopted in many applications, such as aerospace, chemical, oil and gas extraction, power generation, and automotive [1,4,6,11]. The ASTM B446 standard [12] requires alloy 625 to be heat-treated following two processes: soft annealing and solution annealing. The former requires a minimum temperature of 870 °C, and it is recommended for applications below 600 °C, where good mechanical and corrosion properties are required [12]. The latter is instead suggested to improve the creep strength at temperatures above 600 °C, and it is performed at a minimum temperature of 1093 °C [12]. In the soft-annealed condition, this alloy is characterized by an austenitic microstructure with a heterogeneous distribution of primary Nb and Ti carbides and nitrides [8–11,13]. The thermal exposure above about 600 °C during processing, heat treatment, and service can activate complex precipitation phenomena that are able to modify the mechanical and corrosion resistance significantly [1,10]. On the other

hand, special heat treatments can be developed to obtain a hardening effect when required by the service conditions [12]. The time–temperature–precipitation (TTP) curves available in the literature are reported and adapted in Figure 1 for both the conventional alloy and that manufactured by SLM focusing the attention on the δ phase that is the most detrimental for the material's toughness. Metal carbides (MC, M_6C, and $M_{23}C_6$) and intermetallic (especially γ'' phase) and Laves phases can be present as well [10]. These compounds can decrease the corrosion resistance (especially when intergranular Cr- and Mo-rich carbides precipitate in the metal matrix), the ductility (especially when Cr- and Mo-rich carbides are created at the grain boundary), and the deformability of the alloy [1–4,10,14–16]. Finally, niobium, aluminum, and titanium promote the precipitation of the intermetallic hardening γ'' phase.

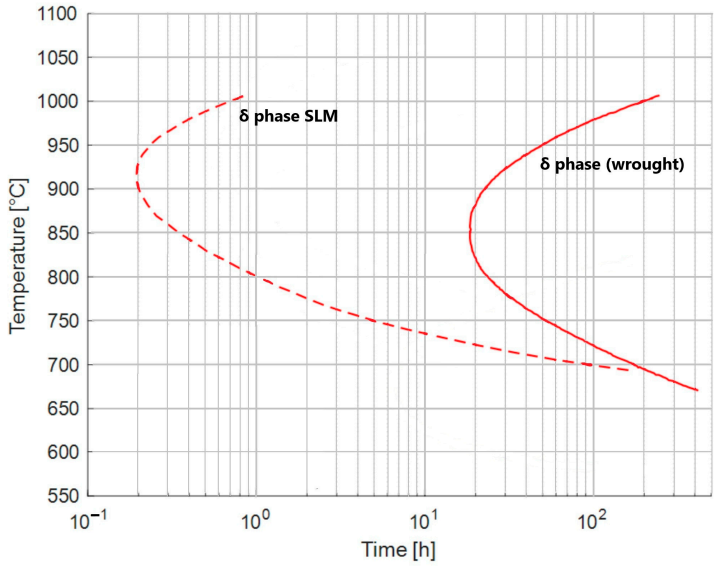

Figure 1. Experimental time–temperature–precipitation (TTP) curves for the delta phase of the SLMed 60 alloy 625 compared to those of the wrought (WR) alloy. Adapted from [10,17,18].

Nowadays, additive manufacturing is increasingly adopted for producing a variety of components especially when complex geometries are required. In fact, in these cases, the conventional manufacturing processes are typically not suitable because of technological limits and/or shape complexity. Among the wide range of additive technologies, this research work is focused on the selective laser melting (SLM) technique. Starting from a CAD model, this method allows us to generate parts layer by layer with a build direction perpendicular to the base plate. Each powder bed is selectively melted by a laser beam. Once the first layer is completed, the base plate is lowered, and the stacking process is continued. During the process, an inert gas (argon or nitrogen) is adopted to avoid powder oxidation within the chamber. Considering the huge growth in the adoption of additive manufacturing techniques in the last decade, this research work is also aimed at investigating the mechanical properties of the selective laser-melted alloy 625 in comparison with those of the conventionally manufactured one. This is extremely useful for designers in the transition from the conventional 625 alloy to the additive manufactured one with reliable data about the mechanical performance and strategies for further strength enhancement based on tailored heat treatments. The literature data about the mechanical properties of the selective laser-melted alloy 625 are reported in Table 1 and compared to those of the conventional wrought and centrifugally cast alloys. Table 2 provides a summary of the data reported in Table 1 with the range and the average values for each condition. According to these data, the as-built selective laser-melted alloy 625 shows outstanding mechanical properties compared to those of the conventional wrought

and centrifugally cast alloys. Moreover, in the as-built condition, the mechanical strength is reduced by both soft- (1038 °C) and solution-annealing (1150 °C) treatments because of grain coarsening after recrystallization and the progressive removal of the original dendritic structure. However, because of the excellent fineness of the as-built microstructure, the mechanical strength upon annealing treatments remains higher than that observed in both the conventional wrought and centrifugally cast alloys. These excellent properties make selective laser melting a promising manufacturing process from the point of view of static mechanical strength.

Table 1. Literature data about the mechanical properties of the selective laser-melted alloy 625 compared to those of the conventional wrought and centrifugally cast alloys. A% is the percentage of elongation.

Condition	Hardness	YS [MPa]	UTS [MPa]	A%	Reference
As-built (SLM)	---	567–783	836–1041	10–57	[19]
As-built (SLM)	---	350–400	840–910	56–62	[20]
As-built (SLM)	285 HBW	618–783	891–1041	33–41	[21,22]
As-built (SLM)	---	770	1039	40	[23]
As-built (SLM)	---	709–859	1103–1242	27–30	[24]
As-built (SLM)	342 HV0.5	566	1087	29	[25]
As-built (SLM)	304 HV0.3	---	---	---	[26]
As-built (SLM)	332 HV0.5	676–767	964–1055	34–42	[27]
As-built (SLM)	273–303 HV2 300–320 HV0.1	630	827	---	[28]
As-built (SLM) + 1038 °C	---	523–577	841–854	---	[19]
As-built (SLM) + 1038 °C	253 HV0.5	598–633	955–1020	39–43	[27]
As-built (SLM) + 1150 °C	---	379	851	55	[22]
As-built (SLM) + 1150 °C	190 HBW	396	883	55	[21]
As-built (SLM) + 1150 °C	190 HBW	---	---	---	[29]
Wrought (solubilized)	---	413	914	70	[30]
Wrought (solubilized)	---	350	809	76	[23]
Wrought (solubilized)	169–275 HV30	317–460	751–910	47–70	[11,31]
Centrifugally cast	80–90 HRB 151–188 HV	290–310	580–595	46–57	[28,32]

Table 2. Summary of the data reported in Table 1 with range and average values for each condition.

Condition		YS [MPa]	UTS [MPa]	YS/UTS [-]	A%
As-built (SLM)	Range	350–859	827–1242	0.43–0.76	10–62
	Average	653	990	0.66	38
As-built (SLM) + 1038 °C	Range	523–633	841–1020	0.62–0.68	39–43
	Average	583	918	0.64	41
As-built (SLM) + 1150 °C	Range	379–396	851–883	0.45–0.45	55–55
	Average	388	867	0.45	55
Wrought (solubilized)	Range	317–460	751–914	0.43–0.47	47–76
	Average	384	851	0.45	68
Centrifugally cast	Range	290–310	580–595	0.50–0.52	46–57
	Average	300	588	0.51	53

The additive manufacturing technique permits a high customization level and design freedom in terms of shape and thicknesses. Such peculiarity is fundamental to efficiently exploit topological optimization at the design stage, with the aim of obtaining improved geometries in terms of weight and mechanical performance. However, low productivity and high manufacturing costs remain critical aspects for a broader application of these techniques. Moreover, in the as-built condition, additively manufactured parts are typically associated with poor surface finishing and process-induced defects which can detrimentally affect the fatigue resistance and lead to incompatibility with geometrical tolerances. For this reason, post-processing techniques, such as hot isostatic pressing, shot peening, sand blasting, electropolishing, and machining, can be adopted to improve the surface quality and the defect content. In the as-built condition, selective laser-melted (SLMed) components are characterized by the presence of textured tracks with their orientation dependent on the scanning strategy. Because the process involves high cooling rates, the microstructure is characterized by melt pools composed of very fine dendritic structures with both columnar and cellular morphology. The cellular morphology is induced by the modification of the columnar one due to high cooling rates [33]. The presence of high solidification rates and several local thermal cycles determines the formation of a very fine microstructure with a high level of micro-segregation [17]. Even though such high cooling rates are able to develop metallic glasses, alloy 625 solidifies as a crystalline solid with the possible formation of metastable phases sometimes with an amorphous structure. According to the literature [34,35], the dendrite cores are mainly enriched with nickel and chromium, while the interdendritic regions are rich in niobium and molybdenum and depleted in chromium. Such enrichment in niobium and molybdenum towards the interdendritic region promotes the formation of the δ and γ'' phases [17]. Therefore, the precipitation response in the selective laser-melted material is significantly enhanced. The comparison among the TTP curves of the conventional and selective laser-melted materials is reported in Figure 1. According to the literature [25], one of the main drawbacks of the SLM process is the formation of thermally induced residual stresses. This phenomenon can determine severe distortion and even failure caused by the accommodation of the residual stresses after the removal of the component from the build plate. Such behavior becomes more and more critical in the presence of thin components. This phenomenon is mainly provoked by the extremely high cooling rates (up to 10^6 K/s) achieved during the SLM process which determine strong thermal gradients between the layers [17]. For this reason, stress-relieving treatment performed before removing the components from the build plate is required to prevent such a detrimental phenomenon. According to the literature [5], the minimum stress-relieving temperature recommended for conventional alloy 625 is 870 °C (1 h per inch of section). In the selective laser-melted material, as observed by several authors [17,18,25], which is different from the wrought alloy, the formation of the detrimental δ, Ni_3Nb phase at 870 °C is obtained after very short exposure times (15 min). The precipitation of this phase provokes a significant decrease in toughness, tensile deformability, and corrosion resistance [25]. In fact, the low chromium content along the Ni_3Nb precipitates of both the γ'' and δ phases creates local anodic regions in the microstructures which are preferentially attacked, leading to an accelerated corrosion rate [36,37]. A further loss in corrosion resistance can be determined by the simultaneous precipitation of chromium-rich carbides that can be obtained at 870 °C after short exposure times, as demonstrated by the TTP diagram in Figure 1. The dramatic toughness loss in the presence of the δ phase is induced by its elongated and needle-shaped morphology. As reported in the literature [29], SLMed alloy 625 shows a faster kinetic of δ-phase precipitation in comparison to the conventional wrought alloy. In fact, in the alloy processed using SLM, at 870 °C, the formation of the δ phase starts after 15 min, while at least 20 h are required for the wrought alloy. Some studies also demonstrate that the presence of residual stresses promotes the precipitation response, but this

effect has a lower importance compared to micro-segregation [17]. Consequently, this research work investigates alternative stress-relieving temperatures that are able to relieve residual stresses, avoid the formation of δ phase, and maintain acceptable mechanical and corrosion properties. As reported by Martucci et al. [25], stress-relieving treatments performed at reduced temperatures in the range from 750 °C to 800 °C prevent the formation of the δ phase, but only a partial reduction (from 50% to 90%) in the residual stresses is obtained. Therefore, this research work investigates the feasibility of higher stress-relieving temperatures in terms of both mechanical and corrosion properties. Considering that the stabilization heat treatment is performed at 980 °C in the conventional wrought alloy [12], we decided to investigate the stress-relieving temperature of 980 °C to also permit a simultaneous improvement in the corrosion resistance, with a clear beneficial industrial effect related to the production of SLM parts with high mechanical resistance and superior corrosion properties.

Starting from the results published in prior research papers of the authors, the aging response of the as-built selective laser-melted material upon single- and double-aging treatments was analyzed in different time–temperature conditions among the most promising alloys by comparing the results against those obtained in the conventional alloy. The mechanical properties were measured using hardness and tensile tests, while corrosion resistance was analyzed in selected conditions in terms of susceptibility to intergranular corrosion in a solution of ferric sulfate and sulfuric acid for 120 h, according to the ASTM G28-A standard [38]. After the investigation of the aging treatment, the stress-relieving temperature was studied to improve the mechanical strength, tensile deformability, and corrosion resistance.

2. Materials and Method

The selective laser-melted alloy 625 was provided in the as-built condition in the form of bars printed horizontally, as shown in Figure 2. The dimensions of the transversal section were 12.5 mm × 12 mm, and the length was equal to 100 mm. The adopted bars were manufactured for each layer using the island scanning strategy, thus forming a chessboard pattern with a layer thickness of 30 µm, and the laser parameters are summarized in Table 3. The printing parameters were optimized by the producer aiming to minimize the residual porosity and improve the mechanical characteristics.

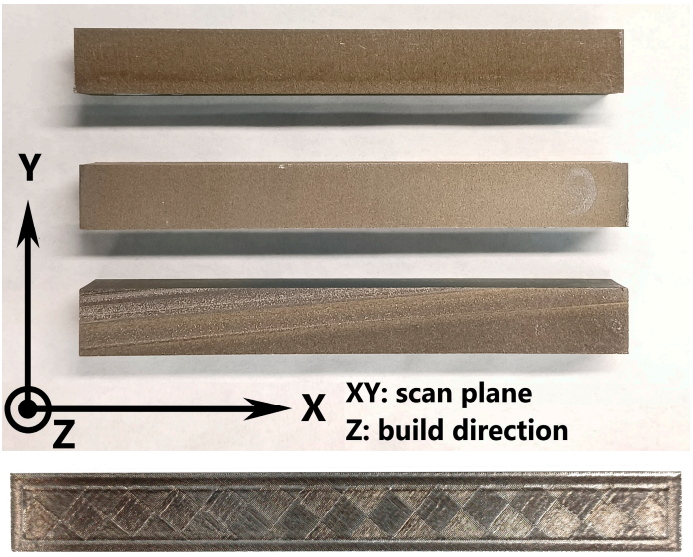

Figure 2. As-built selective laser-melted bars made of alloy 625 adopted in this work. (**a**) View of some of the printed rods; (**b**) details of the island scanning strategy adopted for the inner chessboard pattern.

Table 3. Laser parameters adopted for the contour and the inner area of the SLMed bars.

	Contour	Inner Area (Islands)
Power [W]	120	180
Speed [mm/s]	400	900
Spot size [μm]	50	150

The aging treatments were carried out in a laboratory furnace. The tensile specimens were machined along the longitudinal direction of the bars. The samples for microstructural analyses and hardness tests were prepared according to the conventional metallographic technique. In particular, cutting was performed using silicon carbide wheels with a Remet (model TR100 EV) cutting machine (Bologna, Italy). The mounting of the metallographic samples was performed in hot thermo-setting phenolic resin using a mounting machine. The grinding and polishing operations were performed using a Struers machine (Ballerup, Denmark). Chemical etching was carried out in five parts HCl diluted in one part 30% H_2O_2 for 10 s [5,39,40]. Microstructural analyses were carried out via a Leica light optical microscope (Wetzlar, Germany) and a Zeiss scanning electron microscope (Oberkochen, Germany). The HV30 Vickers hardness tests were conducted using a Wolpert Testor 930 hardness tester (Ludwigshafen am Rhein, Germany) according to the EN ISO 6507 standard [41]. The hardness tests of the selective laser-melted material were performed on the ZX plane. In each tested condition, five hardness measurements were carried out. Tensile tests were performed in selected conditions according to the EN ISO 6892 standard using round proportional specimens (6 mm gauge length and diameter) with an INSTRON 4507 testing machine (Norwood, MA, USA) [42]. The intergranular corrosion tests were carried out in a solution of ferric sulphate and sulfuric acid for 120 h, according to the ASTM G28—Method A standard [38]. The size of the corrosion specimens was 12 mm × 12.5 mm × 8 mm. They were cut along the longitudinal direction of the printed bars; then, they were prepared and polished according to the ASTM G28—Method A standard [38]. The mechanical strength requirements are reported in the ASTM B446 standard [12]. For corrosion resistance, a maximum corrosion rate of 1.20 mm/year was considered since it represents a typical prescription for most of the industrial applications of this grade.

The experimental data on the conventional forged and soft-annealed (1038 °C) alloy 625 were elaborated for comparison purposes from the literature data already published by Panzeri et al. [11,43,44]. In this case, the material was taken from an as-forged 60 mm diameter rod. All the soft-annealing and aging treatments were carried out on the metallographic samples and the tensile and corrosion specimens using a laboratory furnace. The samples for metallographic analyses and hardness tests were cut from the received rod with dimensions of 10 mm × 10 mm × 10 mm. The tensile specimens were machined from the longitudinal direction of the received rod. Hardness, tensile, and corrosion tests were carried out considering the same procedure and the reference standards adopted for the tests on the selective laser-melted material [38,41,42].

3. Results and Discussion

3.1. As-Built and Stress-Relieved Conditions

Figure 3 reports the micrographs of the selective laser-melted material in each plane obtained via light optical and scanning electron microscopy. XY is the scan plane, and it is perpendicular to the build direction Z. In the XY plane, the microstructural analysis showed the presence of elongated tracks of the melt pools with hatch angle rotation in the layer-stacking process equal to 60°, as shown in Figure 3b. The micrographs related

to the ZX and YZ planes report melt pools stacked in the build direction with uniform orientation and shape (Figure 3c,d). The solidified microstructure is represented in the SEM micrographs of Figure 3e,f. Both cellular-shaped structures and elongated dendrites are present with different orientations. The melt pool boundaries are clearly highlighted by the chemical etching process in Figure 3, and they are denoted by dashed yellow lines in the SEM micrographs. The average values of the melt pool width and depth were measured using the micrographs of the as-built material. They resulted equal to 115 µm and 220 µm, respectively.

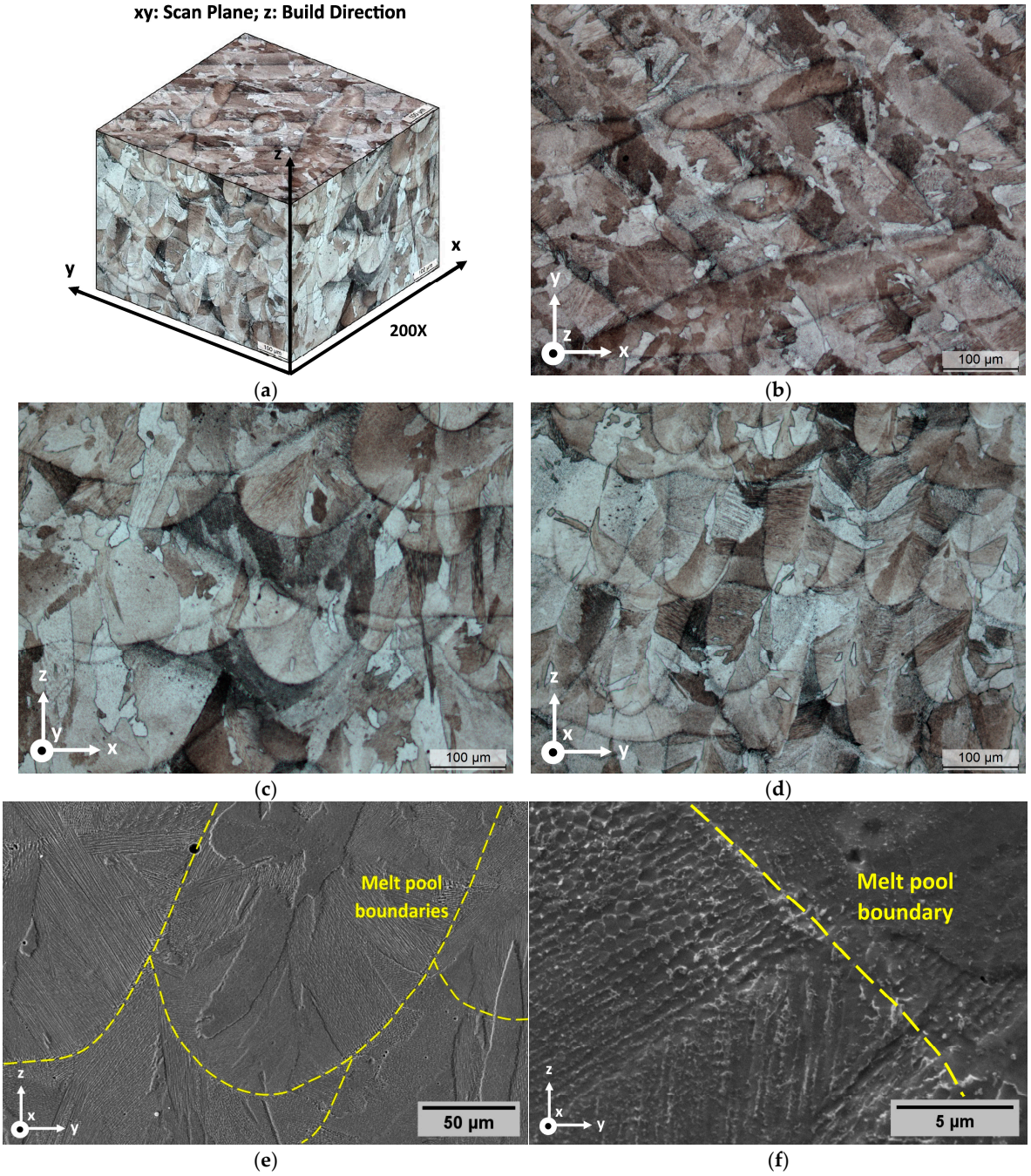

Figure 3. Micrographs of the selective laser-melted material in the as-built condition obtained via light optical and scanning electron microscopy. Figure (**a**) reports an overview of the microstructural features on three perpendicular planes. The melt pools on the three planes are shown in (**b**–**d**). SEM observation of the melt pools are reported in (**e**,**f**): dendrites with different orientations are visible in (**f**).

In SLMed alloy 625, the room-temperature mechanical properties obtained via the hardness and tensile tests in both the as-built and stress-relieved conditions are reported in Tables 4 and 5.

Table 4. Vickers hardness HV30 of the SLMed alloy 625 in both the as-built and stress-relieved conditions for each plane. The standard deviation values range from 1 to 3 HV30.

Plane	As-Built HV30	Stress-Relieved (875 °C 45 min) HV30
XY	312	314
YZ	306	307
ZX	310	311
Average	309	311

Table 5. Room-temperature mechanical properties of the SLMed alloy 625 in both the as-built and stress-relieved conditions. Tensile specimens were machined along the Y direction of the SLMed bars (longitudinal direction). Z% is the percentage reduction in area. The standard deviation values range from 1 to 2% for A% and Z% and from 2 to 10 MPa for YS and UTS.

	As-Built					Stress-Relieved (875 °C 45 min)				
	YS [MPa]	UTS [MPa]	YS/UTS	A%	Z%	YS [MPa]	UTS [MPa]	YS/UTS	A%	Z%
This work	732	1041	0.70	31.0	38	742	1078	0.69	28.0	30
Minimum ASTM B446	414	827	---	30.0	---	414	827	---	30.0	---

In both the as-built and the stress-relieved conditions, the selective laser-melted alloy 625 is characterized by outstanding mechanical strength. In fact, it is significantly higher compared not only with the average literature properties of the conventionally manufactured material reported in Table 2 (wrought and centrifugally cast) but also compared to the minimum requirements defined by the ASTM B446-19 standard [12]. This strength increase is obtained at the expense of tensile deformability, which is reduced when compared to that of the conventional material. Moreover, in the stress-relieved condition, the percentage of elongation after fracture A% is lower than the minimum standard of the prescription. The mechanical properties in the as-built condition are compatible with the literature ranges reported in Table 2 for SLMed alloy 625. The ratio between yield strength and ultimate tensile strength is appreciably increased in the selective laser-melted material (0.70) compared to the literature data of both the wrought (0.45) and centrifugally cast (0.51) counterparts reported in Table 2. In addition, the mechanical performance of the selective laser-melted material is significantly better than that of the centrifugally cast version, as shown by the comparison with the literature data in Table 2.

The susceptibility to intergranular corrosion was determined following the ASTM G-28 Method A standard [38] in both the as-built and stress-relieved conditions. The results were compared with those of the conventional wrought and soft-annealed material. In the as-built condition, the corrosion rate was equal to 0.38 mm/year after the 120 h corrosion test. Therefore, corrosion resistance in this condition is slightly higher than that measured by Panzeri et al. [43] on the conventional wrought and soft-annealed material (0.65 mm/year). Cabrini et al. [33] observed significantly higher corrosion resistance in the as-built condition (0.72 mm/year) compared to that of the conventional wrought and soft-annealed material (1.50 mm/year). They attributed this difference to the very fine dendritic structure of

the selective laser-melted alloy. In the stress-relieved condition, the corrosion rate was equal to 7.07 mm/year. As also reported in the literature [17,18,25,34,45], such a dramatic loss compared to the excellent behavior of the as-built material is mainly determined by the fast precipitation of carbides and the δ phase starting from the interdendritic regions. Consequently, this result confirms that the stress-relieving treatment at the temperature (875 °C) recommended for the conventional alloy is not feasible in the selective laser-melted material because of the significant loss in corrosion resistance induced by its faster precipitation response.

3.2. Single- and Double-Aging Treatments

The age-hardening response upon single-aging treatments was investigated in the selective laser-melted material at the same aging temperatures considered by Panzeri et al. [43,44] for the conventional wrought alloy, i.e., 732 °C and 621 °C. The experimental single-aging curves obtained using the hardness tests are reported in Figure 4 and were compared with those obtained by Panzeri et al. [43,44] on the conventional forged and soft-annealed material. The main difference is related to the initial hardness, which is significantly lower in the forged material (soft-annealed condition) compared to the selective laser-melted one (as-built condition). As previously described, this difference can be ascribed to the improved microstructural fineness in the selective laser-melted alloy. For such a reason, the conventional forged and soft-annealed alloy requires a single aging process at 621 °C for 600 h to attain a hardness value equal to that in the as-built condition for the selective laser-melted material. Regarding the hardness increment, the selective laser-melted material is characterized by a faster response in the early stage of precipitation, especially in the case of single aging at 621 °C. Then, the rate of hardness increase starts reducing compared to the behavior of the conventional material.

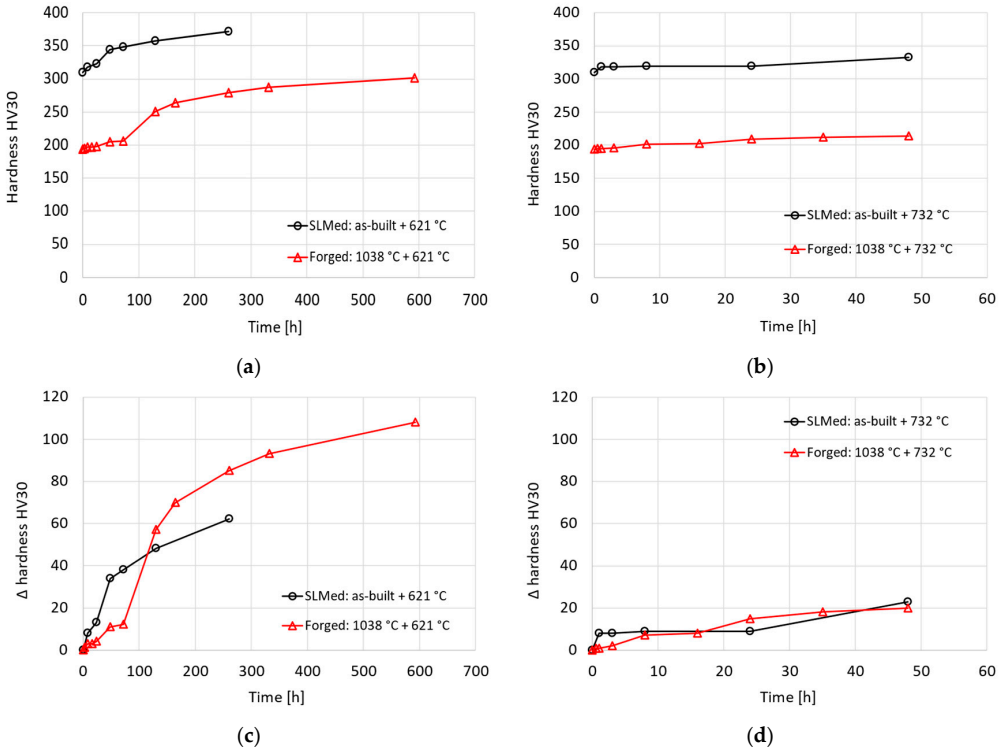

Figure 4. Hardness curves after single-aging treatments at 621 °C (**a**,**c**) and 732 °C (**b**,**d**) of the selective laser-melted alloy in comparison to the conventional forged one. The hardness increase induced by the aging treatment is significantly less for the SLMed specimens, even if their hardness always remains higher than that of the forged material. The standard deviation values range from 1 to 5 HV30.

Successively, starting from the results obtained by Panzeri et al. [43,44] on the double aging of the conventional forged alloy, the double-aging response with primary aging at 732 °C and secondary aging at 621 °C was also investigated in the selective laser-melted material by varying the exposure times at both the temperature levels. The results, reported in Figure 5, were compared to those obtained in the conventional material. Figure 5b shows that the hardness increase allowed for the addition of the primary aging step at 732 °C compared to single aging at 621 °C. According to the results reported in Figure 5b, the acceleration provided by the double-aging procedure is more significant in the conventional forged alloy compared to the selective laser-melted one. In fact, in the latter case, the hardness increment is largely reduced, and this behavior is even more evident when the duration of secondary aging is increased. Therefore, in the selective laser-melted material, the beneficial effects of double aging in terms of mechanical strengthening are appreciably lower than those experimented in the conventional alloy. Such different behavior is probably determined by the faster precipitation response of the additively manufactured material that does not need additional primary aging at higher temperatures to trigger and accelerate the age-hardening process, as is required for the conventional alloy [43,44].

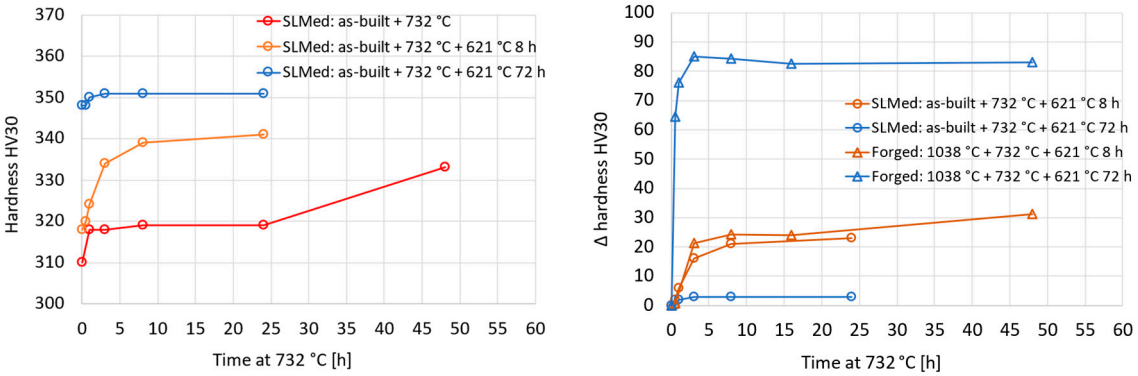

(**a**) (**b**)

Figure 5. (**a**) Hardness curves upon double aging at 732 °C and 621 °C of the selective laser-melted alloy 625 in the as-built condition; (**b**) comparison of the hardness increments with double aging allowed for the addition of primary aging compared to single aging at 621 °C. The standard deviation values range from 1 to 3 HV30.

The influence of the single-aging treatments at 621 °C on room-temperature mechanical strength was investigated via tensile tests for both the selective laser-melted alloy and the conventional forged one. The results are reported and compared in Figure 6. In the conventional material, because of the presence of insufficient mechanical properties in the soft-annealed condition, the aging treatment is required to satisfy the minimum standard requirements [12]. In particular, in this case, single aging at 621 °C for 130 h is associated with acceptable tensile properties. Such strength improvement is obtained at the expense of tensile deformability, which is reduced, but it remains well above the minimum standard requirement (30%) [12]. The selective laser-melted alloy 625 is characterized by excellent mechanical strength in the as-built condition, but the percentage of elongation after fracture A% is very close to the minimum standard requirement [12]. In this case, the aging treatment can be exploited to further improve its mechanical strength. Nevertheless, such a strengthening effect is obtained at the expense of deformability. In fact, for the tested aging conditions, the values of the percentage of elongation after fracture A% are lower than the minimum prescription [12].

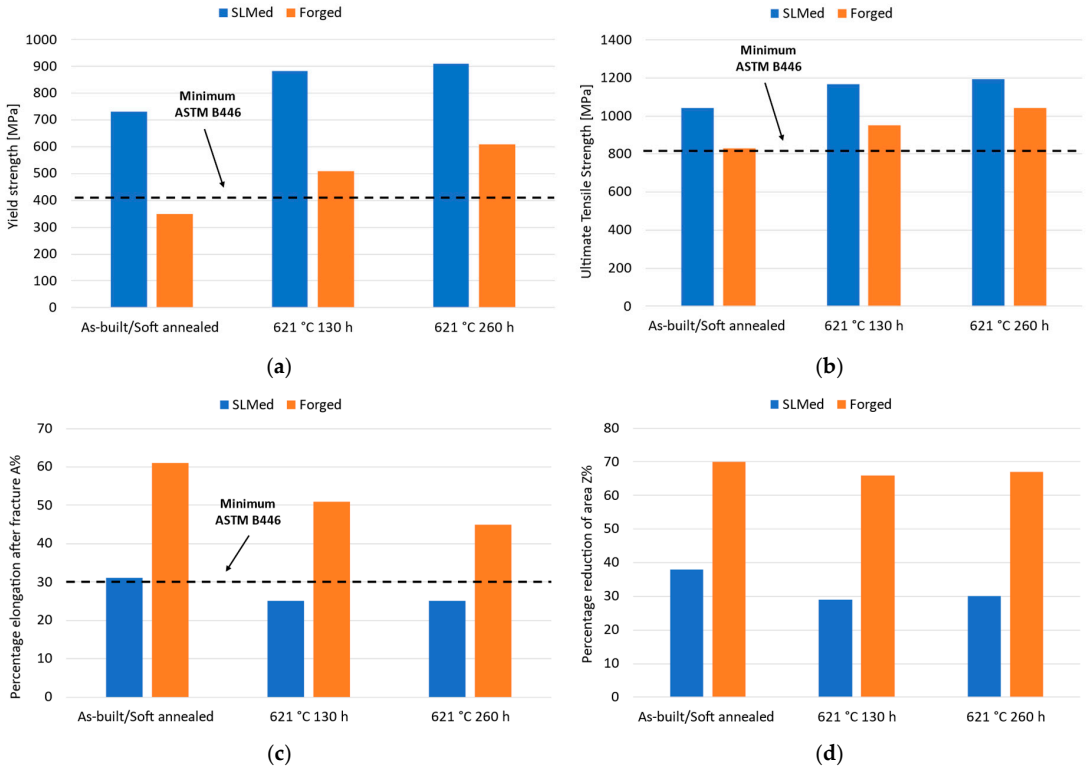

Figure 6. Room-temperature tensile properties after single-aging treatments at 621 °C of the conventional forged and soft-annealed alloy 625 [43,44] and the selective laser-melted one. Figures (**a**,**b**) report the yield strength (**a**) and the ultimate tensile strength (**b**) in selected conditions. The mechanical properties of the as-built material are significantly higher than those of the conventional forged alloy. Figures (**c**,**d**) report the percentage elongation after fracture A% (**c**) and the percentage reduction of area Z% (**d**). Tensile deformability is lower and even below the standard minimum requirement for the aged conditions. The standard deviation values for YS and UTS range from 2 to 13 MPa and from 1 to 2% for A% and Z%.

In the stress-relieved condition (875 °C 45 min), the mechanical properties of the selective laser-melted alloy 625 are similar to those in the as-built condition. However, tensile deformability is lower than the minimum prescription of the ASTM B446 standard [12]. In addition, the corrosion rate determined according to the ASTM G28-Method A standard is well above the limit value considered in this research work [38]. As reported in the literature [17,25,34,35,45], such dramatic degradation of properties is determined by the precipitation of carbides and the δ phase starting from the interdendritic regions and moving towards the dendrite center. Therefore, this behavior confirms that the stress-relieving temperature of 875 °C (recommended for the conventional alloy) is not feasible in the selective laser-melted material because of its faster precipitation response. Also in the conventionally manufactured alloy 625, the formation of the δ phase determines a severe loss of tensile deformability [2], but the precipitation of this embrittling phase requires at least 20 h at 875 °C, according to the time–temperature–precipitation diagram reported in Figure 1. Based on the literature TTP curve shown in Figure 1 for the selective laser-melted alloy 625, the onset of δ phase formation at 875 °C requires only 15 min due to the presence of faster precipitation [17,18]. According to the literature [25], the stress-relieving treatment at 875 °C is suitable to obtain a sufficient mitigation of residual stresses, but at the expense of a severe toughness loss due to δ phase formation. For this reason, it is required to optimize the stress-relieving temperature by avoiding the simultaneous precipitation of detrimental phases. Such microstructural modifications can be avoided with a sufficient reduction in the stress-relieving temperature, but the mitigation of residual stresses can become insufficient [25]. Another possibility is represented

by the adoption of temperatures above 875 °C. In this case, the reduction in residual stresses is ensured, but in order to not activate detrimental microstructural changes, it is necessary to select temperatures far enough from the nose of the TTP curves of the δ phase, which is located at about 920 °C. However, upon increasing the temperature, the loss of mechanical strength due to microstructural recrystallization and coarsening can become significant, and it should be carefully considered in order to identify the condition with the best combination of tensile strength, deformability, and corrosion resistance.

The influence of high-temperature annealing on the mechanical strength of the as-built material was investigated from 980 °C to 1100 °C. According to the results reported in Figure 7, thermal exposure above 875 °C determines a loss in mechanical strength compared to the as-built condition. In particular, at 980 °C and 1038 °C, the reduction in hardness is limited (10% and 15%, respectively), but this loss becomes more significant at 1100 °C (30 %). This reduction in mechanical strength upon high-temperature annealing was investigated via optical microscopy, as shown in Figure 8. By increasing the annealing temperature, the melt pool boundaries and the traces of the prior as-built microstructure become less visible, and they disappear almost completely at 1100 °C. In addition, the presence of recrystallized structures and annealing twins becomes more and more evident up to full recrystallization at 1100 °C, where the microstructural morphology is more similar to that of conventional forgings. This microstructural transformation and subsequent grain coarsening are associated with the loss in mechanical strength upon high-temperature annealing, as confirmed by the literature [19,46].

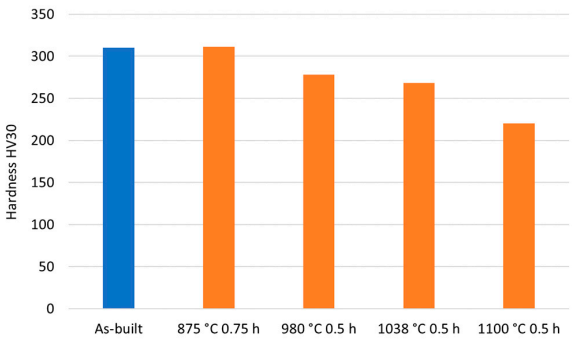

Figure 7. Hardness variation after high-temperature annealing from the as-built condition. It is due to the recrystallization phenomena occurring during the heat treatment. The standard deviation values range from 1 to 3 HV30.

According to the ASTM B446 standard [12], the corrosion resistance of the conventional alloy 625 can be improved by adopting a stabilization heat treatment at 980 °C after the solution-annealing treatment. For this reason and not to excessively reduce the mechanical strength of the as-built material, the temperature of 980 °C was selected as a potential alternative to the stress-relieving temperature of 875 °C. Moreover, according to the time–temperature–precipitation diagram reported in Figure 1, the onset of δ phase formation at 980 °C is delayed compared to that at 875 °C. The feasibility of this alternative temperature was assessed via tensile and corrosion tests. The tensile properties are reported in Figure 9. The selection of the alternative heat treatment at 980 °C for 0.5 h is associated with a slight reduction in tensile strength (15 % for yield strength and 3 % for ultimate tensile strength) compared to the as-built condition. However, the tensile properties remain well above the minimum prescriptions of the ASTM B446 standard [12]. An important advantage of this new temperature is represented by the moderate increase in tensile deformability. In fact, in this case, the percentage of elongation after fracture A% satisfies the minimum standard requirement, while the stress-relieving treatment at 875 °C was associated with insufficient A% values, as shown in Figure 9. In addition, tensile deformability is also slightly improved compared to the as-built condition.

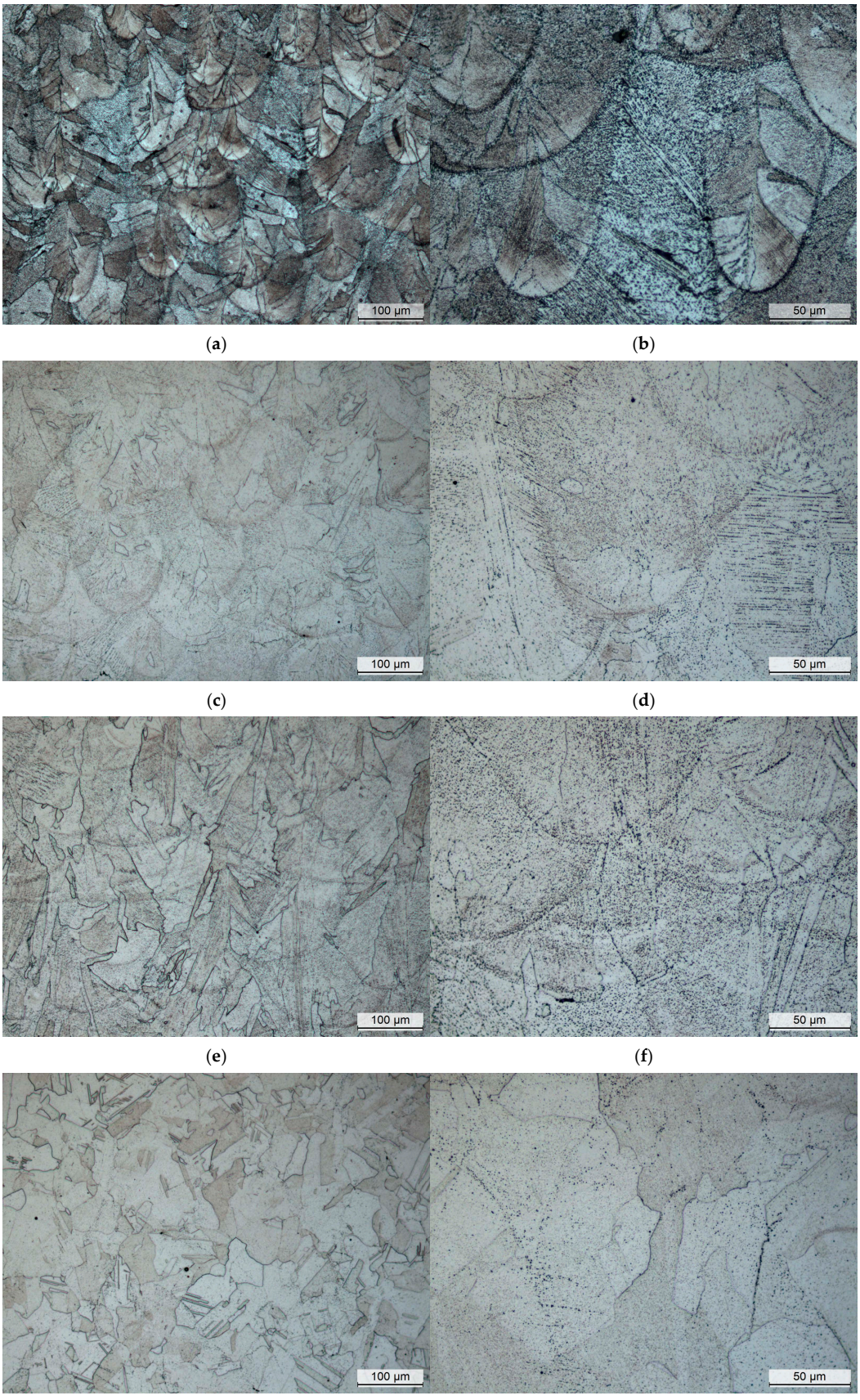

Figure 8. Optical micrographs on the ZY plane at 200X (**a**,**c**,**e**,**g**) and 500X (**b**,**d**,**f**,**h**) of the selective laser melted material after annealing at different temperatures from the as-built condition: (**a**,**b**) 875 °C 45 min; (**c**,**d**) 980 °C 0.5 h; (**e**,**f**) 1038 °C 0.5 h; (**g**,**h**) 1100 °C 0.5 h.

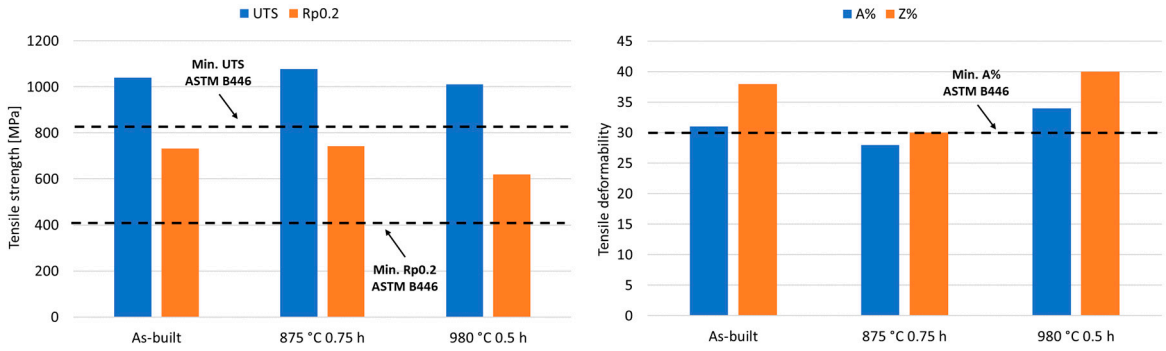

(**a**) (**b**)

Figure 9. Room-temperature tensile strength (**a**) and tensile deformability (**b**) after heat treatment at 980 °C for 0.5 h compared to the as-built condition and to those obtained at the stress-relieving temperature recommended by the standard (875 °C). The mechanical resistance is slightly less than that of the as-built and 850 °C stress-relieved conditions, but the tensile deformability is improved and superior to the minimum standard requirement. The standard deviation values for YS and UTS range from 3 to 12 MPa and up to 1% for A% and Z%.

The susceptibility to intergranular corrosion was investigated following the ASTM G28—Method A standard [38]. The results obtained on the selective laser-melted material were compared with those obtained on the conventional forged alloy 625 published by Panzeri et al. in previous research studies [43,44]. All the experimental results were collected in the performance map reported in Figure 10 relating to the tensile and corrosion properties. In Figure 10, the green shaded area corresponds to the acceptability region with respect to the minimum standard requirements for the tensile properties [12]. Since the minimum yield strength requirement is more critical compared to the ultimate tensile strength one, the values associated with the latter property were not included in the performance map. The data labels report the corrosion rate in mm/year according to the ASTM G28—Method A standard. An acceptable limit for industrial applications of this grade is 1.2 mm/year (green label: acceptable; red label: not acceptable). Corrosion resistance and tensile deformability in the case of stress-relieving treatment at 875 °C are significantly improved after modifying the standard recommended temperature with a higher value, i.e., 980 °C, at the expense of a slight reduction in mechanical strength. Regarding the single-aging treatment at 621 °C, the strengthening effect is obtained with a detrimental reduction in corrosion resistance. Similarly, in conventional forged alloy 625, the increase in mechanical strength by aging treatment reduces both tensile deformability and corrosion resistance. In this case, full acceptability is obtained in a very narrow region, as also demonstrated by our previous research studies [43,44]. For this reason, considering the strict requirement for the corrosion resistance and rapid degradation of this property upon aging, the exploitation of aging treatments is significantly limited, and it requires a careful optimization of the aging time. Such limitation is even more critical in the selective laser-melted material because of its faster precipitation response. In this case, an additional obstacle to the adoption of aging treatments is represented by the rapid loss of the tensile deformability below the minimum standard requirement.

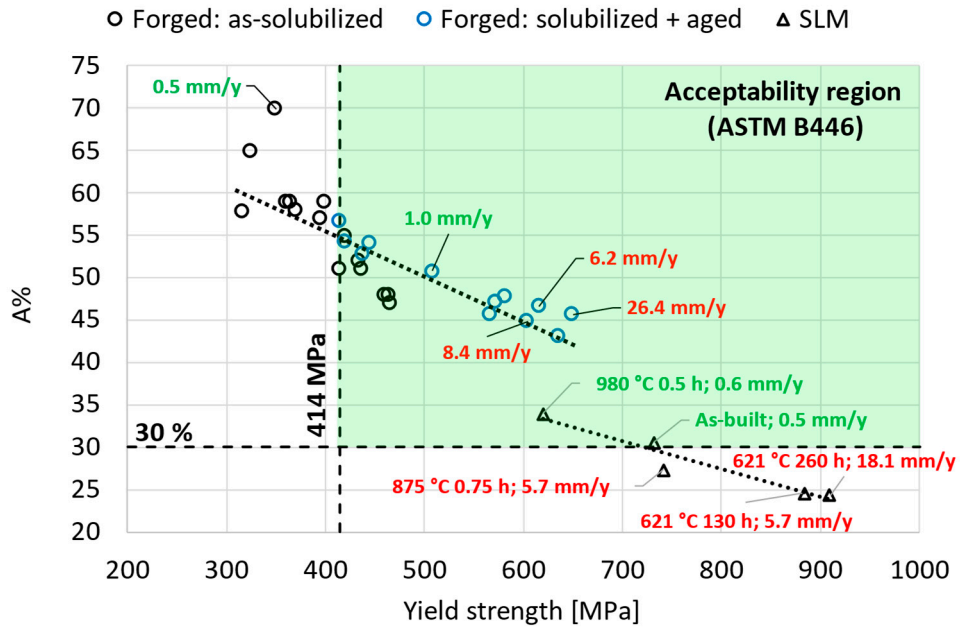

Figure 10. Performance map relating the tensile and corrosion properties of the conditions tested in this work for the selective laser-melted material and in our previously published papers [43,44] for conventional forged alloy 625. The green shaded area corresponds to the acceptability region with respect to the minimum standard requirements for the tensile properties (ASTM B446 [12]). The data labels report the corrosion rate in mm/year according to the ASTM G28—Method A standard [38] (green label: acceptable; red label: not acceptable). The standard deviation values range from 2 to 14 MPa for YS and from 1 to 2% for A%.

The corroded profiles were investigated in selected conditions for having a relationship with the corrosion rates and characterize the corrosion mechanism. The melt pool boundaries of the laser tracks are preferentially corroded compared to the inner regions. This behavior is confirmed by the literature data, which address such selective attack to the enhanced precipitation of sensitizing Ni_3Nb phases in these zones [33,36,47]. The corrosion rates are in good agreement with the observed corroded profiles.

Figure 11 shows some sections of the specimens subjected to the corrosion tests cut perpendicularly to the surfaces exposed to the corroding solution. Figure 11a,b represent the as-built condition. Some residual porosity is visible, but no corrosion damage characterizes the surface. The corresponding corrosion rate is in fact very low (0.5 mm/year). Pictures c and d are instead related to specimens aged at 621 °C for 130 h. Unlike the as-built condition, the surface clearly shows the effects of the corroding solution. The corrosion attack follows the laser tracks' borders preferentially, even if the damage includes the inner zones as well. Accordingly, the corrosion rate (5.7 mm/year) was much higher than of the as-built one. The effect of the standard stress-relieving temperature (850 °C) on corrosion resistance is clearly detrimental, as shown in Figure 11e,f. Similarly to the aged condition, the corrosion damage proceeds along the laser track direction and removes material both from the border and the inner part of the track. Also, in this case, the corrosion rate is quite high (5.7 mm/year). Finally, the new heat treatment at 980 °C resulted in a corrosion rate (0.6 mm/year) very similar to the as-built one. The corrosion pits reported in Figure 11g,h were in fact very small on all the corroded surface.

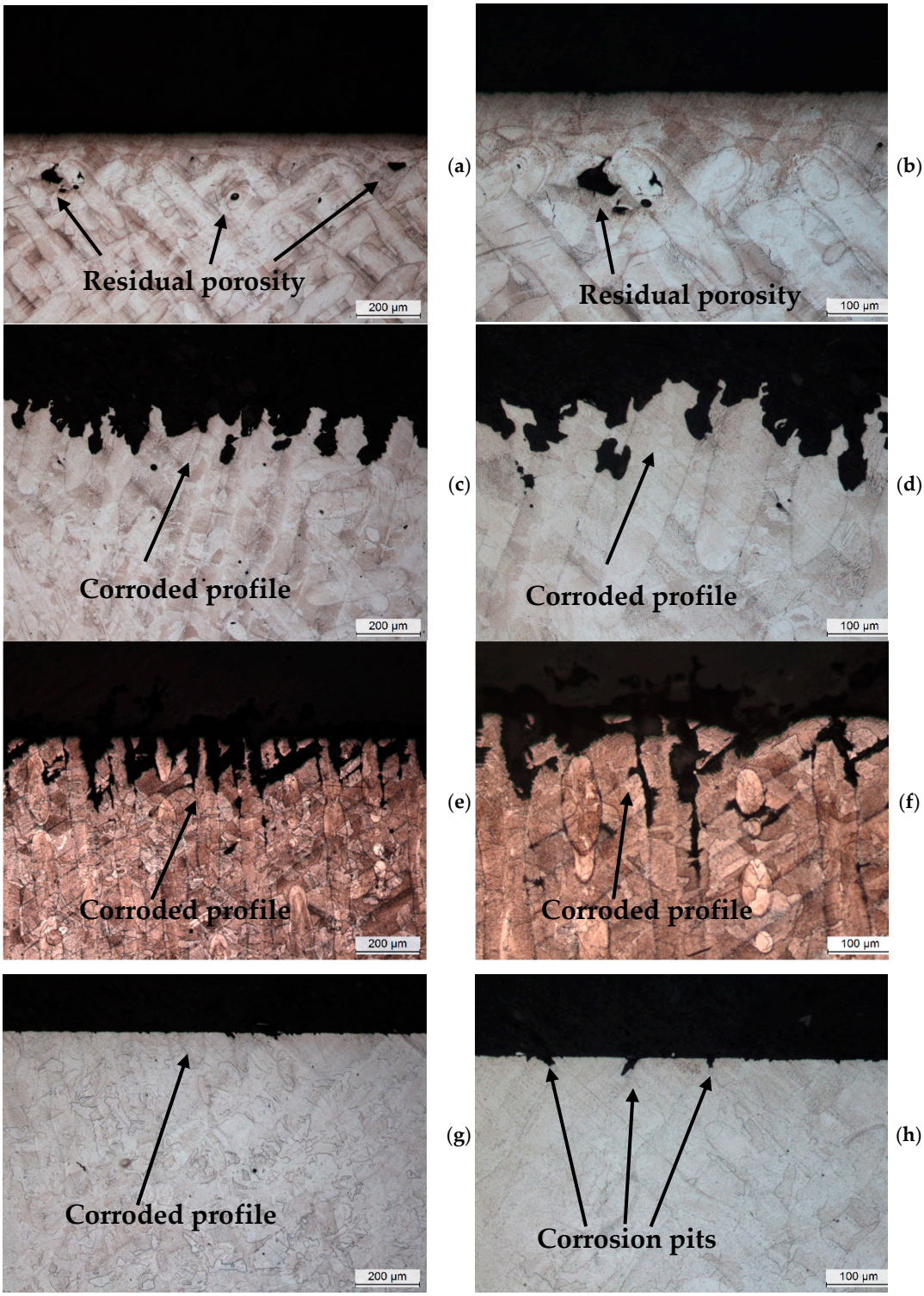

Figure 11. Metallographic sections of the scan plane of selected corrosion specimens. (**a**,**b**) As-built: 0.5 mm/year; (**c**,**d**) 621 °C 130 h: 5.7 mm/year; (**e**,**f**) 875 °C 0.75 h: 5.7 mm/year; (**g**,**h**) 980 °C 0.5 h: 0.6 mm/year.

4. Conclusions

The selective laser-melted alloy 625 shows outstanding mechanical and corrosion properties in the as-built condition. Compared to the conventional forged alloy, this difference is the most significant, and it can be ascribed to the improved microstructural fineness of the selective laser-melted material. However, because of the high local thermal gradients induced by the SLM process, residual stresses are present, and their mitigation by suitable

stress-relieving treatment is normally required to avoid distortions and failures when the component is removed from the build plate, especially in the presence of thin components. The conventional forged alloy 625 is stress-relieved at a minimum temperature of 870 °C. However, at this temperature, the selective laser-melted material is characterized by the very rapid precipitation of the δ phase which detrimentally degrades the deformability and corrosion resistance after short exposure times. Such different behavior depends on the fact that the aging response of the selective laser-melted alloy is significantly accelerated compared to that of the conventional material because of the higher micro-segregation level and the presence of residual stresses. Lower stress-relieving temperatures are not suitable for a satisfying mitigation of residual stresses. For this reason, in this research work, considering the TTP diagram of this alloy, higher stress-relieving temperatures were analyzed by investigating the influence on the mechanical and corrosion properties. In particular, the adoption of a higher temperature, i.e., 980 °C for 0.5 h, allows us to mitigate residual stresses while maintaining acceptable corrosion resistance. This alternative temperature also permits us to improve tensile deformability, which becomes even better than that in the as-built condition. This is one of the most important findings of this work, since the new stress-relieving treatment at 980 °C guarantees an optimal compromise among tensile properties, deformability, and corrosion resistance. This result is particularly important from a practical point of view, since it allows for the production of SLM parts with high mechanical properties that are superior to the minimum standard requirements even if slightly lower than those of the as-built condition and improved corrosion properties.

Even though the selective laser-melted material is characterized by excellent mechanical properties, this work investigates the possibility of a further strength improvement by single- and double-aging treatments starting from previous results obtained for the conventional forged alloy. Regarding the single-aging treatments at 732 °C and 621 °C, compared to the conventional material, a faster precipitation response is obtained in the early stages of formation. On the other hand, the acceleration provided by the double-aging procedure is much more significant in the conventional forged alloy. In fact, in the selective laser-melted material subjected to double-aging treatments, the hardness increments are largely reduced, and this behavior is even more evident when the duration of secondary aging is increased. Therefore, in the selective laser-melted alloy, the beneficial effects of double aging are appreciably lower than those in the conventional alloy. Furthermore, considering that the tensile deformability is already close to the minimum standard prescription in the as-built condition, the adoption of aging treatments encounters some limitations because of deformability loss which is typically associated with the strengthening effect of intermetallic precipitates. In fact, for the tested aging conditions, the values of the percentage of elongation after fracture A% are lower than the minimum standard requirement. In addition, as already observed in the conventional forged alloy 625, the reduction in corrosion resistance upon aging treatments is another critical aspect which is even more significant compared to the conventional material because of the faster precipitation response observed in the additively manufactured grade.

Author Contributions: Conceptualization, B.R., R.G. and D.P.; methodology, B.R., R.G. and D.P.; formal analysis, B.R., R.G. and D.P.; investigation, B.R., R.G. and D.P.; writing—original draft preparation, D.P.; writing—review and editing, B.R., R.G. and D.P.; supervision, B.R. and R.G. All authors have read and agreed to the published version of the manuscript.

Funding: This research received no external funding.

Institutional Review Board Statement: Not applicable.

Informed Consent Statement: Not applicable.

Data Availability Statement: The dataset is available upon request from the authors.

Conflicts of Interest: The authors declare no conflicts of interest.

References

1. Suave, L.M.; Cormier, J.; Villechaise, P.; Soula, A.; Hervier, Z.; Bertheau, D.; Laigo, J. Microstructural Evolutions During Thermal Aging of Alloy 625: Impact of Temperature and Forming Process. *Metall. Mater. Trans. A* **2014**, *45*, 2963–2982. [CrossRef]
2. Shankar, V.; Bhanu Sankara Rao, K.; Mannan, S.L. Microstructure and Mechanical Properties of Inconel 625 Superalloy. *J. Nucl. Mater.* **2001**, *288*, 222–232. [CrossRef]
3. Sukumaran, A.; Gupta, R.K.; Anil Kumar, V. Effect of Heat Treatment Parameters on the Microstructure and Properties of Inconel-625 Superalloy. *J. Mater. Eng. Perform.* **2017**, *26*, 3048–3057. [CrossRef]
4. Heubner, U.; Kloewer, J.; Alves, H.; Behrens, R.; Schindler, C.; Wahl, V.; Wolf, M. *Nickel Alloys and High-Alloyed Special Stainless Steels: Properties-Manufacturing-Applications*, 4th ed.; Expert-Verlag: Renningen, Germany; Stuttgart, Germany, 2012.
5. ASM International. *ASM Specialty Handbook: Nickel, Cobalt, and Their Alloys*; Davis, J., Ed.; ASM International: Materials Park, OH, USA, 2000.
6. Donachie, M.J.; Donachie, S.J. *Superalloys: A Technical Guide*, 2nd ed.; ASM International: Materials Park, OH, USA, 2002.
7. Eiselstein, H.L.; Tillack, D.J. The Invention and Definition of Alloy 625. In *Proceedings on Superalloys 718, 625, and Derivatives*; Loria, E.A., Ed.; The Minerals, Metals & Materials Society: Warrendale, PA, USA, 1991; pp. 1–14.
8. Durand-Charre, M. *The Microstructure of Superalloys*, 1st ed.; Routledge: London, UK, 1968.
9. Patel, S.J.; Smith, G.D. The Role of Niobium in Wrought Precipitation-Hardened Nickel-Base Alloys. In *Proceedings on Superalloys 718, 625, 706 and Derivatives*; Loria, E.A., Ed.; The Minerals, Metals & Materials Society: Warrendale, PA, USA, 2005; pp. 135–154.
10. Floreen, S.; Fuchs, G.E.; Yang, W.J. The Metallurgy of Alloy 625. In *Superalloys 718, 625, 706 and Derivatives*; The Minerals, Metals & Materials Society: Warrendale, PA, USA, 1994; pp. 13–37.
11. Rivolta, B.; Boniardi, M.V.; Gerosa, R.; Casaroli, A.; Panzeri, D.; Pizetta Zordão, L.H. Alloy 625 Forgings: Thermo-Metallurgical Model of Solution-Annealing Treatment. *J. Mater. Eng. Perform.* **2022**, *32*, 5785–5797. [CrossRef]
12. *ASTM B446-19*; Standard Specification for Nickel-Chromium-Molybdenum-Columbium Alloy (UNS N06625), Nickel-Chromium-Molybdenum-Silicon Alloy (UNS N06219), and Nickel-Chromium-Molybdenum-Tungsten Alloy (UNS N06650) Rod and Bar. ASTM International: West Conshohocken, PA, USA, 2019.
13. Reed, R.C.; Rae, C.M.F. Physical Metallurgy of the Nickel-Based Superalloys. In *Physical Metallurgy*; Elsevier: Amsterdam, The Netherlands, 2014; pp. 2215–2290. [CrossRef]
14. Vernot-Loier, C.; Cortial, F. Influence of Heat Treatments on Microstructure, Mechanical Properties and Corrosion Behaviour of Alloy 625 Forged Rod. In *Proceedings on Superalloys 718, 625, and Derivatives*; Loria, E.A., Ed.; The Minerals, Metals & Materials Society: Warrendale, PA, USA, 1991; pp. 409–422.
15. Heubner, U.; Köhler, M. Effect of Carbon Content and Other Variables on Yield Strength, Ductility, and Creep Properties of Alloy 625. In *Proceedings on Superalloys 718, 625, 706 and Derivatives*; Loria, E.A., Ed.; The Minerals, Metals & Materials Society: Warrendale, PA, USA, 1994; pp. 479–488.
16. Heubner, U.; Köhler, M. The Effect of Final Heat Treatment and Chemical Composition on Sensitization, Strength and Thermal Stability of Alloy 625. In *Superalloys 718, 625, 706 and Derivatives*; The Minerals, Metals & Materials Society: Warrendale, PA, USA, 1997; pp. 795–803.
17. Lindwall, G.; Campbell, C.E.; Lass, E.A.; Zhang, F.; Stoudt, M.R.; Allen, A.J.; Levine, L.E. Simulation of TTT Curves for Additively Manufactured Inconel 625. *Metall. Mater. Trans. A* **2019**, *50*, 457–467. [CrossRef] [PubMed]
18. Stoudt, M.R.; Lass, E.A.; Ng, D.S.; Williams, M.E.; Zhang, F.; Campbell, C.E.; Lindwall, G.; Levine, L.E. The Influence of Annealing Temperature and Time on the Formation of δ-Phase in Additively-Manufactured Inconel 625. *Metall. Mater. Trans. A* **2018**, *49*, 3028–3037. [CrossRef]
19. Sitek, R.; Ciftci, J.; Moszczyńska, D.; Maj, P.; Ura-Bińczyk, E.; Warzybok, P.; Cieślik, I.; Wiśniewski, P.; Mizera, J. Effect of Annealing on the Microstructure and Properties of IN 625 Specimens Manufactured by Selective Laser Melting. *Arch. Civil. Mech. Eng.* **2022**, *22*, 207. [CrossRef]
20. Gonzalez, J.A.; Mireles, J.; Stafford, S.W.; Perez, M.A.; Terrazas, C.A.; Wicker, R.B. Characterization of Inconel 625 Fabricated Using Powder-Bed-Based Additive Manufacturing Technologies. *J. Mater. Process Technol.* **2019**, *264*, 200–210. [CrossRef]
21. Marchese, G.; Lorusso, M.; Parizia, S.; Bassini, E.; Lee, J.-W.; Calignano, F.; Manfredi, D.; Terner, M.; Hong, H.-U.; Ugues, D.; et al. Influence of Heat Treatments on Microstructure Evolution and Mechanical Properties of Inconel 625 Processed by Laser Powder Bed Fusion. *Mater. Sci. Eng. A* **2018**, *729*, 64–75. [CrossRef]
22. Marchese, G.; Bassini, E.; Parizia, S.; Manfredi, D.; Ugues, D.; Lombardi, M.; Fino, P.; Biamino, S. Role of the Chemical Homogenization on the Microstructural and Mechanical Evolution of Prolonged Heat-Treated Laser Powder Bed Fused Inconel 625. *Mater. Sci. Eng. A* **2020**, *796*, 140007. [CrossRef]

23. Lee, J.; Terner, M.; Jun, S.; Hong, H.-U.; Copin, E.; Lours, P. Heat Treatments Design for Superior High-Temperature Tensile Properties of Alloy 625 Produced by Selective Laser Melting. *Mater. Sci. Eng. A* **2020**, *790*, 139720. [CrossRef]
24. Chen, F.; Wang, Q.; Zhang, C.; Huang, Z.; Jia, M.; Shen, Q. Microstructures and Mechanical Behaviors of Additive Manufactured Inconel 625 Alloys via Selective Laser Melting and Laser Engineered Net Shaping. *J. Alloys Compd.* **2022**, *917*, 165572. [CrossRef]
25. Martucci, A.; Marchese, G.; Bassini, E.; Lombardi, M. Effects of Stress-Relieving Temperature on Residual Stresses, Microstructure and Mechanical Behaviour of Inconel 625 Processed by PBF-LB/M. *Metals* **2023**, *13*, 796. [CrossRef]
26. Luna, V.; Trujillo, L.; Gamon, A.; Arrieta, E.; Murr, L.E.; Wicker, R.B.; Katsarelis, C.; Gradl, P.R.; Medina, F. Comprehensive and Comparative Heat Treatment of Additively Manufactured Inconel 625 Alloy and Corresponding Microstructures and Mechanical Properties. *J. Manuf. Mater. Process.* **2022**, *6*, 107. [CrossRef]
27. Renishaw. In625-0402 Powder for Additive Manufacturing: Data Sheet. September 2017. Available online: https://www.renishaw.com/media/pdf/en/674a7fa1d94b4da3907f9a2275b6f46d.pdf (accessed on 18 January 2023).
28. Concli, F.; Gerosa, R.; Panzeri, D.; Fraccaroli, L. High- and Low-Cycle-Fatigue Properties of Additively Manufactured Inconel 625. *Progress. Addit. Manuf.* **2024**, *9*, 1921–1940. [CrossRef]
29. Marinucci, F.; Marchese, G.; Bassini, E.; Aversa, A.; Fino, P.; Ugues, D.; Biamino, S. Hardness Evolution of Solution-Annealed LPBFed Inconel 625 Alloy under Prolonged Thermal Exposure. *Metals* **2022**, *12*, 1916. [CrossRef]
30. Kim, K.-S.; Kang, T.-H.; Kassner, M.E.; Son, K.-T.; Lee, K.-A. High-Temperature Tensile and High Cycle Fatigue Properties of Inconel 625 Alloy Manufactured by Laser Powder Bed Fusion. *Addit. Manuf.* **2020**, *35*, 101377. [CrossRef]
31. Rivolta, B.; Gerosa, R.; Tavasci, F.; Ori Belometti, L. Mechanical and Microstructural Characterization of Forged Inconel 625 Ring Gaskets for Oil and Gas Application. *Mater. Perform. Charact.* **2017**, *6*, 20170030. [CrossRef]
32. Rivolta, B.; Gerosa, R.; Tavasci, F.; Ori Belometti, L. Metallurgical Analysis of Inconel 625 Metallic Gaskets Produced by Centrifugal Casting. *Mater. Perform. Charact.* **2017**, *6*, 20170036. [CrossRef]
33. Cabrini, M.; Lorenzi, S.; Testa, C.; Brevi, F.; Biamino, S.; Fino, P.; Manfredi, D.; Marchese, G.; Calignano, F.; Pastore, T. Microstructure and Selective Corrosion of Alloy 625 Obtained by Means of Laser Powder Bed Fusion. *Materials* **2019**, *12*, 1742. [CrossRef]
34. Lass, E.A.; Stoudt, M.R.; Williams, M.E.; Katz, M.B.; Levine, L.E.; Phan, T.Q.; Gnaeupel-Herold, T.H.; Ng, D.S. Formation of the Ni3Nb δ-Phase in Stress-Relieved Inconel 625 Produced via Laser Powder-Bed Fusion Additive Manufacturing. *Metall. Mater. Trans. A* **2017**, *48*, 5547–5558. [CrossRef] [PubMed]
35. Dubiel, B.; Sieniawski, J. Precipitates in Additively Manufactured Inconel 625 Superalloy. *Materials* **2019**, *12*, 1144. [CrossRef]
36. Tawancy, H.M.; Allam, I.M.; Abbas, N.M. Effect of Ni3Nb Precipitation on the Corrosion Resistance of Inconel Alloy 625. *J. Mater. Sci. Lett.* **1990**, *9*, 343–347. [CrossRef]
37. Zhu, Z.; Sui, Y.; Dai, A.; Cai, Y.; Xu, L.-L.; Wang, Z.; Chen, H.; Shao, X.; Liu, W. Effect of Aging Treatment on Intergranular Corrosion Properties of Ultra-Low Iron 625 Alloy. *Int. J. Corros.* **2019**, *2019*, 9506401. [CrossRef]
38. *ASTM G28-02*; Standard Test Methods for Detecting Susceptibility to Intergranular Corrosion in Wrought, Nickel-Rich, Chromium-Bearing Alloys. ASTM International: West Conshohocken, PA, USA, 2015.
39. Carpenter Technology Corporation. CarTech® Custom Age 625 PLUS® Alloy: Technical Datasheet. Available online: www.carpentertechnology.com/alloy-finder/625-Plus (accessed on 25 August 2020).
40. Carpenter Technology Corporation. A Guide to Etching Specialty Alloys for Microstructural Evaluation. Available online: https://carpentertechnology.com/blog/a-guide-to-etching-specialty-alloys (accessed on 14 November 2023).
41. *ISO 6507-1:2018*; Metallic Materials—Vickers Hardness Test. BSI Standards: London, UK, 2018.
42. *BS EN ISO 6892-1:2019*; Metallic Materials—Tensile Testing. BSI Standards Limited: London, UK, 2020.
43. Rivolta, B.; Gerosa, R.; Panzeri, D.; Nazim, A. Optimization of the Mechanical and Corrosion Resistance of Alloy 625 through Aging Treatments. *Crystals* **2024**, *14*, 139. [CrossRef]
44. Rivolta, B.; Gerosa, R.; Panzeri, D. Influence of Single- and Double-Aging Treatments on the Mechanical and Corrosion Resistance of Alloy 625. *Metals* **2024**, *14*, 823. [CrossRef]
45. Lass, E.A.; Stoudt, M.R.; Katz, M.B.; Williams, M.E. Precipitation and Dissolution of δ and Γ″ during Heat Treatment of a Laser Powder-Bed Fusion Produced Ni-Based Superalloy. *Scr. Mater.* **2018**, *154*, 83–86. [CrossRef]
46. Li, C.; White, R.; Fang, X.Y.; Weaver, M.; Guo, Y.B. Microstructure Evolution Characteristics of Inconel 625 Alloy from Selective Laser Melting to Heat Treatment. *Mater. Sci. Eng. A* **2017**, *705*, 20–31. [CrossRef]
47. Dinda, G.P.; Dasgupta, A.K.; Mazumder, J. Laser Aided Direct Metal Deposition of Inconel 625 Superalloy: Microstructural Evolution and Thermal Stability. *Mater. Sci. Eng. A* **2009**, *509*, 98–104. [CrossRef]